Determination of material models for arterial walls from uniaxial extension tests and histological structure

Gerhard A. Holzapfel

Determination of material models for arterial walls from uniaxial extension tests and histological structure

Gerhard A. Holzapfel

An approach is proposed that allows the determination of material models from uniaxial tests and histostructural data including fiber orientation of the tissue. A combination of neo Hookean and Fung type strain energy functions is utilized, and inequality constraints imposed on the constitutive parameters are derived providing strict local convexity and preferred fiber orientations. It is shown how the Fung type model gets a pseudo structural aspect inherent in the phenomenological model; a correlation between the fiber structure and the parameters of the Fung type model is explicitly provided. In order to apply the proposed approach, quasi static uniaxial extension tests of preconditioned prepared strips from the intima, media and adventitia of a human aorta with non atherosclerotic intimal thickening are acquired in axial and circumferential directions; structural information from histological analyses for each aortic tissue are documented. Data reveal a remarkable thickness, load bearing capacity and stiffness of the intimal samples in comparison with the media and adventitia. Constitutive parameters for each aortic tissue layer are determined by solving the constrained problem using a penalty function method; a new approach for the estimation of appropriate start values is proposed. Finally, the predictivity and efficacy of the material models is shown by comparing model data with data from the uniaxial extension tests and histological image analyses.

Soft biological tissue; Artery; Aorta; Uniaxial extension test; Histology; Fiber reinforced material; Constitutive model; Nonlinear constrained optimization

1. Introduction

Uniaxial extension tests of soft biological tissue strips are not sufficient for the determination of multi-dimensional (two or three-dimensional) material models that aim to predict the material behavior in physiological loading states. One essential reason for this is that the 'experimental paths' of uniaxial extension tests with respect to the in-plane strain components do not cover the physiological domain. Fig. 1, for example, shows a schematic plot indicating the 'experimental paths' for uniaxial extension of two arterial strips with orientations orthogonal to each other (x_1 denotes the circumferential and x_2 the axial directions of an artery, and convex contours represent states of constant energy of a hypothetical strain-energy function). In addition, Fig. 1 shows the physiological strain domain (indicated by the grey area), which is typically covered by an artery under physiological loading conditions, i.e. cyclic inflation, axial extension (and twist), leading to positive Green–Lagrange strains E_{11} and E_{22} (and stresses) in the circumferential and axial directions. As can be seen, the strain domain in a physiological loading state, does not coincide with the experimental paths obtained from uniaxial extension tests. Since data are provided only for a small domain in the strain space, fitting of multi-dimensional constitutive (material) models to uniaxial data may lead to ill-conditioned equations, slow convergence rates and non-unique solutions. In other

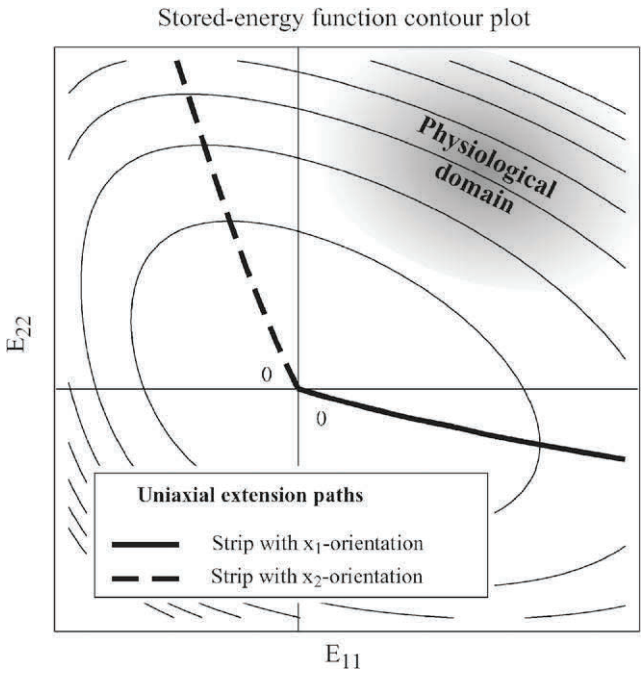

Fig. 1. Schematic plot indicating the Green Lagrange strains E_{11} and E_{22} in the (x_1, x_2) plane, where x_1 denotes the circumferential and x_2 the axial directions of an artery. The convex contours represent states of constant energy of a (hypothetical) strain energy function. Experi mental paths for uniaxial extension of two strips with orthogonal orientations are shown by solid and dashed thick lines.

words, various sets of constitutive parameters may provide equally good representations of uniaxial data but predict material responses for physiological loading states that differ significantly. This problem can be overcome by preparing tissue samples amenable to multi-axial loading, i.e. patches and cylindrical tubes, and simulating in vivo loading states by means of appropriate testing equipment. Frequently, however, such equipment and skilled operators are not available. Moreover, and even more importantly, for many biological specimens such as components of diseased arteries, only (small) strip preparations are feasible. For such cases, consideration of additional information coming, for example, from structural investigations, may help to reduce the variability and to improve the predictive capability of constitutive models.

The objective of this paper is to present an approach that allows reasonable determination of material responses for arterial walls that uses data from uniaxial extension tests. Methods used are based on the constitutive theory of finite hyperelasticity, that utilize a combination of neo-Hookean and Fung-type strain-energy functions. The basic idea of the proposed approach is to impose physically and structurally motivated constraints on the constitutive parameters, and to present a *pseudo-structural* aspect inherent in the phenomenological Fung-type model, i.e. (mean) orientation of collagen and smooth muscle components. For the purpose of comparison, structural information from histological analyses and uniaxial extension tests for the intima, media and adventitia of one human aorta with non-atherosclerotic intimal thickening are acquired, and used to show the predictivity and efficacy of the material model.

2. Methods

2.1. Theoretical framework

The considered type of flat arterial tissue layer is assumed to be a fiber-reinforced material with relatively stiff collagenous fibers embedded in a homogeneous isotropic (soft) ground matrix. The sheet is embedded in a reference frame (right-handed) of coordinate axes with a fixed set of orthonormal basis vectors $\{\mathbf{e}_1, \mathbf{e}_2, \mathbf{e}_3\}$. Suppose that the axes are aligned with the major faces of the sheet and that the fibers lie in the plane spanned by the vectors $\mathbf{e}_1$ and $\mathbf{e}_2$ (notation is adopted from Holzapfel (2000) throughout the paper). The collagenous fibers are organized in two families, which are symmetrically arranged with respect to the x_1- and x_2-axes and which have the same stiffness (x_1 and x_2 denote the circumferential and the axial directions of the artery, respectively). The fiber families are assumed to have preferred orientations characterized by the (mean) fiber angles φ and $-\varphi$ with respect to the x_1-axis. It is these orientations that render the material properties orthotropic. The structural model assumptions are summarized in Table 1. This particular 'histo-structural' design provides the typical orthotropic response observed in a large number of soft biological tissues, such as layers of tube organs (blood vessels, esophagus, gut, ureter, etc.), serous membranes (pericardium, pleura, peritoneum) etc. Note that it is assumed that the orientations of the axes x_1 and x_2 are known a priori.

2.1.1. Kinematics of uniaxial extension tests

Consider two rectangular strips cut out from the flat arterial tissue layer undergoing uniaxial tensile testing.

Table 1
Model assumptions

Structure	Isotropic (soft) ground matrix Two embedded families of (stiff) collagenous fibers Symmetrical fiber arrangement in the (x_1, x_2) plane Fiber angles φ and φ Homogeneous composition
Material	Strain energy function $\Psi = \hat{\Psi}_{iso}(E_{11}, E_{22}) + \hat{\Psi}_{ortho}(E_{11}, E_{22})$; a possible choice for the mechanical response of arterial walls

One strip is aligned with the x_1-axis, while the other is aligned with the x_2-axis. In-plane components E_{11} and E_{22} of the Green–Lagrange strain tensor $\mathbf{E}$ and the (tensile) component of the second Piola–Kirchhoff stress tensor $\mathbf{S}$ is computed from original data. Uniaxial test data appear as characteristic 'experimental paths' in the (E_{11}, E_{22})-plane, as can be seen in Fig. 1. For uniaxial loading the components of the stress tensor that are oriented in the transverse direction of the tensile axis are zero. Therefore, the experimental path must cross the contours of an associated strain-energy function at positions where the transverse component of the second Piola–Kirchhoff stress tensor vanishes.

2.1.2. Constitutive model

The passive mechanical behavior of the considered type of material is characterized by a strain-energy function per unit reference volume, Ψ say, according to Holzapfel and Weizsäcker (1998), i.e.

$$\Psi = \Psi_{iso}(\mathbf{E}) + \Psi_{ortho}(\mathbf{E}), \tag{1}$$

where Ψ_{iso} is an isotropic contribution to Ψ, which governs mainly the initial stiffness of the artery wall represented by the elasticity of the non-fibrous substances (extracellular aqueous ground substance matrix containing proteoglycans and non-cytoskeletal intracellular components). The strain energy Ψ_{ortho} denotes an orthotropic contribution which governs the much higher stiffness at large strains represented by the *randomly oriented* collagen (primarily of type I in the adventitia and intima, and of type III in the media (von der Mark, 1981)) and *aligned* components of collagenous fibers.

As a particular choice for Ψ, the study of Holzapfel and Weizsäcker, 1998, proposed a combined polynomial-exponential form. They suggest to use the neo-Hookean model $\Psi_{iso} = \mu(I_1 - 3)/2$ for the isotropic contribution, with the stress-like material parameter $\mu > 0$ (i.e. the shear modulus), and the first invariant $I_1 = \operatorname{tr}\mathbf{C} = 2\operatorname{tr}\mathbf{E} + 3$ of the right Cauchy–Green tensor $\mathbf{C} = 2\mathbf{E} + \mathbf{I}$, with the unit tensor $\mathbf{I}$.

Assuming incompressibility ($\det \mathbf{C} = 1$), the strain-energy function $\hat{\Psi}(E_{11}, E_{22})$ can be expressed in terms of the Green–Lagrange strain components E_{11} and E_{22}. Thus, $\hat{\Psi} = \hat{\Psi}_{iso}(E_{11}, E_{22}) + \hat{\Psi}_{ortho}(E_{11}, E_{22})$ (see Table 1), with

$$\hat{\Psi}_{iso} = \frac{\mu}{2}\{2(E_{11} + E_{22}) + [(2E_{11} + 1)(2E_{22} + 1)]^{-1} - 1\}. \tag{2}$$

For the orthotropic contribution $\hat{\Psi}_{ortho}$ we adopt an exponential 'Fung-type' strain-energy function which incorporates the four constitutive parameters C, c_{11}, c_{12}, c_{22} (Fung et al., 1979; von Maltzahn et al., 1984; see Holzapfel et al. (2000) for a discussion and a comparative study with other material models, and Holzapfel et al. (1996) for a detailed numerical realization of $\hat{\Psi}_{ortho}$). Thus,

$$\hat{\Psi}_{ortho} = C[\exp(Q) - 1],$$
$$Q = c_{11}E_{11}^2 + c_{12}E_{11}E_{22} + c_{22}E_{22}^2, \tag{3}$$

where $C > 0$ is a stress-like material parameter, whereas the other three are non-dimensional parameters. Consistent with the assumptions about the fiber orientations, $\hat{\Psi}_{ortho}$ is a two-dimensional model expressed in terms of E_{11} and E_{22}. It is a well-established type of strain-energy function describing transverse isotropy in plane, which is frequently used for the representation of nonlinear anisotropic soft biological tissue responses.

Since we may set the stress component $S_{33} = 0$, without loss of generality, we have simply the (non-vanishing) second Piola–Kirchhoff stresses (see, for example, Ogden, 2003)

$$S_{11} = \frac{\partial\hat{\Psi}(E_{11}, E_{22})}{\partial E_{11}}, \quad S_{22} = \frac{\partial\hat{\Psi}(E_{11}, E_{22})}{\partial E_{22}}. \tag{4}$$

Formulation (3) is inherently limited to specific kinematics, for example, it is not suitable for analysis of the through-thickness stress distribution in an artery or for the treatment of shearing deformations. Note, however, that for isochoric deformations without shearing, no approximation is involved in Eq. (3), and therefore the model is three-dimensional despite its two-dimensional form (see also Section 4.2.1 in Holzapfel et al. (2000)). Model (3) can be used to simulate the deformation in special cases, such as that corresponding to simple tension, as studied in the present work, and inflation of an artery regarded as a thin-walled (or thick-walled) circular cylindrical tube.

2.1.3. Inequality constraints

At this point the common approach is to fit the chosen constitutive model to experimental data utilizing nonlinear regression analysis. For the case of uniaxial data, however, the solutions (constitutive parameters) obtained will be questionable, as mentioned in the Introduction. Determination of appropriate inequality constraints restricts the solutions to a small and meaningful domain in the 'parameter space', here spanned by the set $\{\mu, C, c_{11}, c_{12}, c_{22}\}$ of constitutive parameters.

In the following physically and structurally motivated constraints are derived by using the notion of strict local convexity of the strain-energy function $\hat{\Psi}$, which means that the matrix containing the second derivative of $\hat{\Psi}$ with respect to E_{11} and E_{22} is positive definite. This implies that the contours of constant $\hat{\Psi}$ are convex, and, in particular, that the projections of these contours in the (E_{11}, E_{22})-plane are convex, as can be seen in Fig. 2. Convexity is a fundamental physical requirement which ensures physically meaningful and unambiguous mechanical behavior also important from the point of view of numerical computations. It precludes undesirable

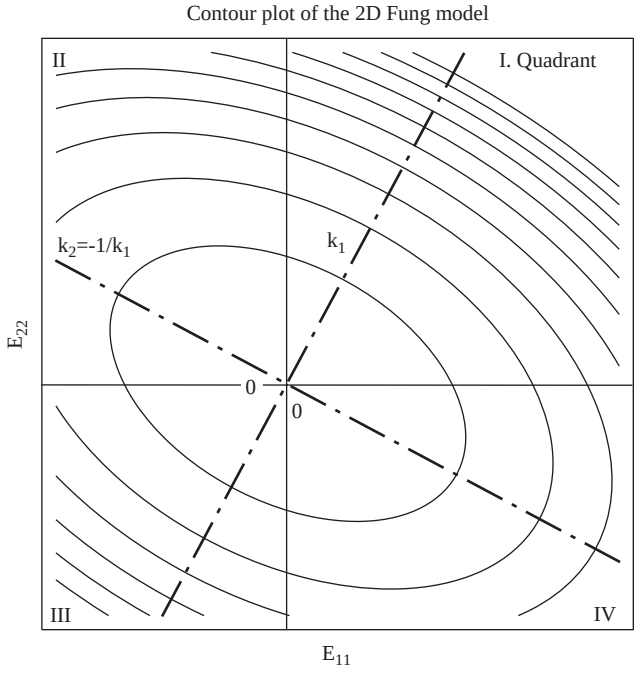

Fig. 2. Contour plots representing states of constant energy of the function (3), as proposed by Fung et al. (1979), with a set of material parameters chosen to illustrate convexity. The eigenvectors with slopes k_1 and $k_2 = 1/k_1$ are indicated by dash dotted lines. Roman numbers I IV denote the quadrants of the (E_{11}, E_{22}) plane.

material instabilities (for a general discussion of convexity and material stability in hyperelasticity the reader is referred to, for example, Ogden (1997), for an application to models in arterial wall mechanics see the comparative study (Holzapfel et al., 2000) and the lecture note (Ogden, 2003)).

Hence, considering Eq. $(3)_2$, the contours may be obtained by setting $Q = const$. Because of the quadratic nature of Q we may write Eq. $(3)_2$ in a matrix form, with the eigenvalues $\gamma_{1,2} = \frac{1}{2}[c_{11} + c_{22} \pm \sqrt{c_{12}^2 + (c_{11} - c_{22})^2}]$, $\gamma_1 > \gamma_2$, of the Hessian matrix. If we require that the Hessian matrix is positive definite, then all eigenvalues are (real and) positive, which implies the inequality

$$4c_{11}c_{22} - c_{12}^2 > 0. \tag{5}$$

This inequality dictates that c_{11} and c_{22} are either positive or negative. Since negative values of c_{11} and c_{22} lead to negative stress components for tensile strains we require that

$$c_{11} > 0, \quad c_{22} > 0. \tag{6}$$

Restrictions (5) and (6) imposed on the material parameters of the two-dimensional Fung model (Fung et al., 1979) were first provided in Holzapfel et al. (2000) (compare with Section 4.2.3 therein). Basically, inequality (5) allows positive and negative values for c_{12}. It turns out, however, that only a positive value is consistent with mechanics, as briefly shown. The eigenvector (principal axis) related to the larger eigenvalue γ_1 is located in the first and third quadrants of the (E_{11}, E_{22})-plane (see Fig. 2), which is the domain for biaxial extension (first quadrant) and compression (third quadrant), respectively. Only then the stress components are positive for all biaxial extensions, and negative for all biaxial compressions. The slope $k_1 = E_{22}/E_{11}$ of the eigenvector related to γ_1 can then be computed by means of standard algebra. Thus,

$$k_1 = \frac{c_{12}}{c_{11} - c_{22} + \sqrt{c_{12}^2 + (c_{11} - c_{22})^2}}, \tag{7}$$

where the root is nonnegative by definition. The location of the eigenvector in the first and third quadrants requires that k_1 must be positive. According to Eq. (6) this is only satisfied if $c_{12} > 0$.

Consequently, the two-dimensional exponential form proposed by Fung et al. (1979) is not convex for all possible sets of material parameters. Function (3) is strictly locally convex *if and only if* certain restrictions are imposed on the material parameters (for a summary of the a priori restrictions on the material parameters see Table 2—'mechanics'). Hence, the material parameters cannot be chosen arbitrarily if convexity of function (3) is desired. Note that in a paper by Wilber and Walton (2002), it is shown that, for example, the strong ellipticity condition, crucial in avoiding certain types of non-physical singularity a priori, imposes very severe restrictions on the material constants in the model (3). In fact, these restrictions are inconsistent with the ability of the model to fit the experimental data.

We assume now that the slope k_1 of one eigenvector (related to γ_1) coincides with the slope $\tan\varphi$ of the (mean) direction of one family of collagen (or smooth muscle component), where the parameter φ is the angle between the (mean) fiber orientation and the circumferential direction of the artery (for a motivation of this assumption see the remark at the end of this section). Thus, we may write

$$k_1 = \tan\varphi. \tag{8}$$

Since the eigenvectors of ellipses are mutually orthogonal the slope k_2 of the second eigenvector is $-1/k_1$ (see Fig. 2). Substituting Eq. (8) in Eq. (7) gives an equation that relates the constitutive parameters c_{11}, c_{12} and c_{22} to the fiber angle φ. After some algebra we deduce that

$$\frac{c_{12}}{c_{11} - c_{22}} = \tan 2\varphi. \tag{9}$$

Hence, knowing that $c_{12} > 0$ this relation implies immediately that $0 < \varphi < \pi/4$ for $c_{11} > c_{22}$, and $\pi/4 < \varphi < \pi/2$ for $c_{22} > c_{11}$.

If the distribution of the fiber angles in a tissue is known from structural investigation, c_{12} can be re-

Table 2
Inequality constraints

Mechanics	$\mu>0,\ C>0,\ c_{11}>0,\ c_{12}>0,\ c_{22}>0$ $4c_{11}c_{22}\quad c_{12}^2>0$ (convexity)
Structure	$\tan 2\varphi_u(c_{11}\quad c_{22})\geqslant c_{12}\geqslant \tan 2\varphi_l(c_{11}\quad c_{22})$ (fiber orientation φ, see Eqs. (9) and (10))

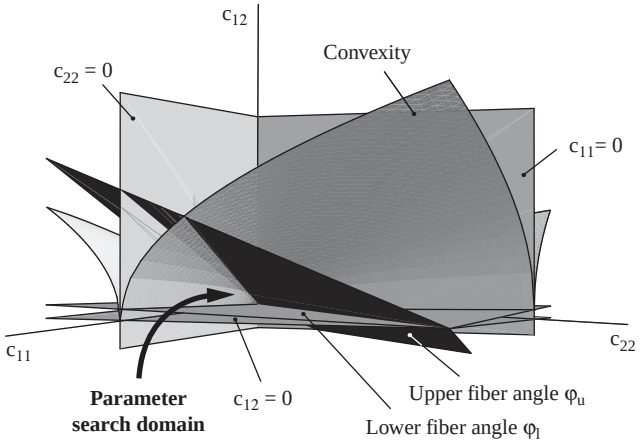

Fig. 3. Sketch of the parameter subspace $\{c_{11}, c_{12}, c_{22}\}$ with related inequality constraints (compare also with Table 2).

stricted according to

$$\tan 2\varphi_u(c_{11}-c_{22})\geqslant c_{12}\geqslant \tan 2\varphi_l(c_{11}-c_{22}), \tag{10}$$

where φ_l and φ_u are appropriate (lower and upper) limits for the fiber angle (φ_l and φ_u could be chosen, for example, as the mean fiber angle $\pm$ standard deviation; Holzapfel et al., 2002). The determined inequality constraints are summarized in Table 2. They restrict the 'search domain' for the constitutive parameters. The constraints may be visualized as boundary surfaces in the 'parameter space' or subspaces of it, as illustrated in Fig. 3.

Note that the slope k_1 of the eigenvector characterizes the path in the (E_{11}, E_{22})-plane perpendicular to the surface of constant energy. Clearly, this path is associated with the maximum fiber stretch λ_f. For the type of considered fiber-reinforced model (Table 1), an analytical expression for the fiber stretch λ_f in terms of φ is given by the kinematic relation (Holzapfel and Gasser, 2001)

$$\lambda_f^2=\lambda_1^2\cos^2\varphi+\lambda_2^2\sin^2\varphi, \tag{11}$$

where λ_1 and λ_2 are the in-plane stretches related to the x_1- and x_2-directions, respectively. They are defined as the ratios of the actual to the unloaded (referential) in-plane specimen dimension.

Remark 1. By intuition we would think that collagen fibers, which somehow 'reinforce' biological tissues in order to bear (higher) loads, naturally grow in that direction in which the maximum stresses (or strains) occur. Hence, collagen fiber directions evolve such that the load-bearing capacity of the tissue is optimized.

In the recent paper, Menzel (2005) developed a theoretical and computational framework that describes the remodeling (isotropic and anisotropic growth and reorientation processes) of biological tissues, considered as transversely isotropic materials. The author has used the property that the stored energy in an anisotropic material takes on an extremum only if the principal axes of stress and strain coincide (see, for example, the early work Pedersen, 1989). In Menzel (2005) it is further shown that the principal axes of stress and strain coincide if the anisotropy axis shares its direction with one of the principal strain directions, which motivates to align the fiber direction with the eigenvector of the strain (see also Driessen et al., 2004). A few representative numerical examples illustrate the alignment of the fiber direction with respect to the predominant principal strain direction during a certain loading process and time interval. Note, however, that a stress-based remodeling concept of the collagen fibers would also have its merits. The collagen fiber direction would then be associated with the directions of the two largest principal (tensile) Cauchy stresses, because it is the high tensile stress domain in which the collagen fibers are mainly active. There is still a debate over which is the superior hypothesis.

3. Example

In order to illustrate the merits of the proposed approach, the determination of layer-specific constitutive models for a human aorta with non-atherosclerotic intimal thickening is demonstrated.

3.1. Specimen preparation and uniaxial extension tests

Since the preparations of intact separated aortic patches or intact (leak-free) tubes of the adventitia, media and the intima suitable for biaxial tests are difficult (or in the case of tubes even impossible) to perform we have prepared strips of aortic tissue. In particular, an abdominal aorta from a human cadaver (female, 80 years, primary disease: congestive cardiomyopathy) was excised during autopsy within 24 h from death. The vessel exhibited no appreciable disease. The heterogeneous arterial wall structure was separated anatomically into its three layers (intima, media,

adventitia). From each arterial layer, strip samples with axial and circumferential orientations were cut out so that six specimens, two for each layer, were obtained. Two black colored chips of a straw were glued transversely in parallel onto the middle part of the samples to act as gage markers for the axial deformation measurements. The length/width ratio was about 6 such that it is most likely that the desired homogeneous stress–strain state within the measuring range could be achieved. For representative tissue samples see, for example, Fig. 4 in Holzapfel et al. (2004a). The strips underwent cyclic uniaxial extension tests in 0.9% NaCl solution at 37 °C with continuous recording of tensile force, gage length and strip width at a constant crosshead speed of 1 mm/min. Gage length and width were measured optically using a PC-based (CPU 586) videoextensometer (model ME 46-350, Messphysik) utilizing a full-image charge-coupled device (CCD) camera, that allowed automatic gage mark and edge recognition. The corresponding deformation data were averaged with respect to the measuring zone and sent to a data-processing unit in real time. For details on the customized tensile testing machine the reader is referred to Schulze-Bauer et al. (2002) and Holzapfel et al. (2004a). Executing five successive loading cycles preconditioned the samples. Typical (free) sample length and width were 30 mm and 5 mm, respectively. Mean thicknesses of intimal, medial and adventitial samples were 0.33, 1.32 and 0.96 mm, whereas a customized back light device was used for measuring the thickness from the lateral sample contour (Schulze-Bauer et al., 2002).

3.2. Histology

After all tests, the strip samples were inserted into a 4% buffered formaldehyde solution (pH 7.4) for fixation and further histological preparation with Elastica van Gieson (EvG). Specimens were embedded maintaining their planar geometry and sectioned serially at 3 μm in tangential orientation so that the fiber orientations in the (x_1, x_2)-plane were seen on the histological images, where x_1 and x_2 denote the circumferential and the axial directions (see Fig. 4). A skilled histopathologist measured the orientation of 60 representative collagen fibers in the intima and adventitia and oblate nuclei of smooth muscle cells in the media per specimen from the histological images. Mean (fiber) angles and standard deviations were determined numerically from the data by assuming normal distribution and symmetrical arrangement with respect to the circumferential direction.

3.3. Optimization

Fitting the material model to experimental data is achieved by optimizing (minimizing) the stress-based

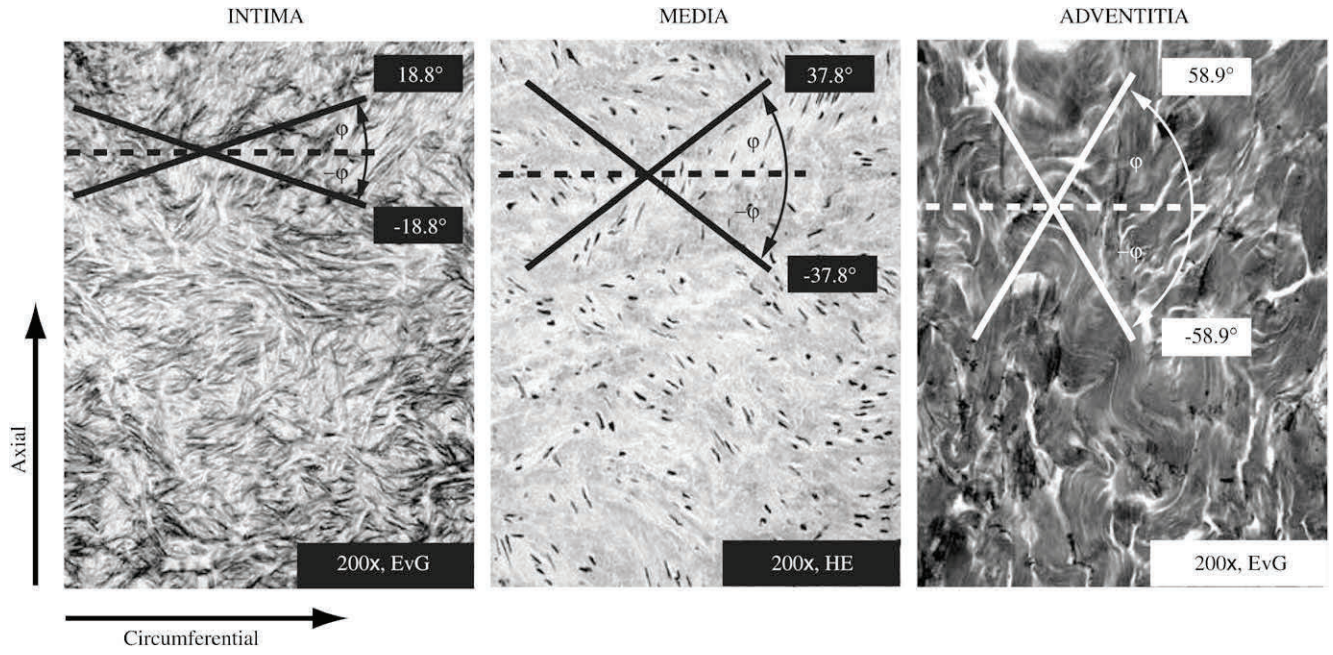

Fig. 4. Histological images (3 μm thick sections) of an intimal strip, a medial strip and an adventitial strip with circumferential orientation (images are contrast enhanced). Planar sectioning was performed so that the in plane fiber orientations are seen. Collagen fibers appear as relatively straight lines in the intima and as wavy structures in the adventitia (only the global orientations of the wavy structures were considered for the determination of the adventitial fiber orientations). In the media oblate nuclei of smooth muscle cells, which appear as black dashes or dots, depending on their orientations and radial positions, indicate preferred orientations of the tissue. Crossing solid lines indicate mean (fiber) orientation characterized by φ (determination of φ is based on additional microphotographs not shown here). EvG, Elastica van Gieson staining. HE, hematoxylin and eosin staining.

nonlinear function

$$f_s = \sum_{i=1}^{n} \left[w_1 \left(\left. \frac{\partial \hat{\Psi}(E_{11}, E_{22})}{\partial E_{11}} \right|_{(i)} - S_{11}^{(i)} \right)^2 + w_2 \left(\left. \frac{\partial \hat{\Psi}(E_{11}, E_{22})}{\partial E_{22}} \right|_{(i)} - S_{22}^{(i)} \right)^2 \right], \tag{12}$$

where n is the number of experimental data records, w_1 and w_2 are weighting factors, and $\partial\hat{\Psi}/\partial E_{11}|_{(i)}$ and $\partial\hat{\Psi}/\partial E_{22}|_{(i)}$ are the second Piola–Kirchhoff stresses related to the x_1- and x_2-directions (see Eq. (4)) and predicted by the constitutive model for the ith data record. For this purpose the in-plane strains $E_{11}^{(i)}$ and $E_{22}^{(i)}$ are computed according to $E_{11}^{(i)} = (\lambda_1^{2(i)} - 1)/2$ and $E_{22}^{(i)} = (\lambda_2^{2(i)} - 1)/2$, with the measured in-plane stretches $\lambda_1^{(i)}$ and $\lambda_2^{(i)}$ for the ith data record. The related 'experimental' second Piola–Kirchhoff stresses $S_{11}^{(i)}$ and $S_{22}^{(i)}$ are calculated directly from the original data as $F/(A\lambda_{tens})$, where F is the actual axial force, A the unloaded cross-sectional area, and the 'experimental' stretch in the tensile direction λ_{tens} is the ratio of the actual gage length to the gage length in the reference configuration. Accordingly, λ_{tens} is either λ_1 or λ_2 depending on the orientation of the sample. Representative sets of 20 data records per sample were extracted from the original data files, whereas data of the loading and unloading branches were averaged.

Alternatively to the stress-based approach expressed by Eq. (12), an energy-based nonlinear function, f_w say, may also be chosen. Thus,

$$f_w = \sum_{i=1}^{n} (\hat{\Psi}^{(i)} - \hat{W}^{(i)})^2, \tag{13}$$

where $\hat{\Psi}^{(i)}$ is the strain energy for the ith data record predicted by the constitutive model, and $\hat{W}^{(i)}$ is the work done by the stress field on the continuum body of unit volume during the stress-free configuration and the current (final) configuration associated with the ith data record. In regard to the theoretical framework introduced in Section 2.1 we may write for the case of hyperelastic properties

$$\hat{W}^{(i)} = \int_0^{E_{11}^{(i)}} S_{11}^{(i)} \, \mathrm{d}E_{11}^{(i)} + \int_0^{E_{22}^{(i)}} S_{22}^{(i)} \, \mathrm{d}E_{22}^{(i)}, \tag{14}$$

where $E_{11}^{(i)}$, $E_{22}^{(i)}$ are the (in-plane) Green–Lagrange strains for the ith data record. The integrals in Eq. (14) are to be computed numerically for each data record by means of polynomial interpolation.

From a mathematical point of view both approaches are equivalent since there is an analytical relation between a strain-energy function and the associated stresses. For this study the stress-based approach (Eq. (12)) is used in order to maximize the accuracy with respect to the representation of stress responses of the uniaxial test data. An additional advantage of the stress-based approach over the energy-based approach is that the weighting factors for the stress components S_{11} and S_{22} allow a better control over the fitting procedure. In contrast to the stress-based approach the energy-based approach tends to smooth the material response because it is based on an integral formulation.

As described in Section 2.1, the neo-Hookean contribution $\hat{\Psi}_{iso}$ to the overall strain energy may be mainly associated with the response of non-fibrous substances. The orthotropic contribution $\hat{\Psi}_{ortho}$ to $\hat{\Psi}$, however, is thought to be the energy mainly stored in the collagenous fibers (Roach and Burton, 1957), which are active at high arterial pressures. Because of this model assumption and the (two-term) potential (1) it is preferable to fit $\hat{\Psi}_{iso}$ separately to a selected subset of data records representing the *initial* isotropic (soft) response of the individual arterial layer. For this purpose the stress–strain curve of the arterial layer strip is divided into low and high stiffness regions. The 'transition point', (E^{trans}, S^{trans}) say, between the two regions is defined as that point of the stress–strain curve with the maximum normal distance to the global secant, which is defined as the line spanned between the origin to the end of the curve (see Fig. 5). Hence, the transition point is located somewhere at the 'knee' of the stress–strain curve. Note that the transition point, as defined here, may not be viewed as an intrinsic material property of the arterial tissue. The transition point depends on the choice of the maximum stress, and the region of the low (nearly linear) modulus which, in general, might also differ between circumferential and axial strips. Anyway, although a rough estimation, for many cases the transition point may serve as a convenient initial measure for the fitting purpose (see also the considerations in the appendix). Best-fit parameters for $\mu > 0$ according to model (2) are determined by means of the Levenberg–Marquardt algorithm. Consequently, μ is no longer a free parameter. It remains to fit the remaining material parameters to the experimentally observed response of the arterial layers.

The goal is now to minimize the nonlinear function (12) subject to the given inequality constraint functions $\phi_m(C, c_{11}, c_{12}, c_{22}) > 0$, where $m \in \{1, 2, 3, \ldots, M\}$ denotes the mth constraint and M is the total number of constraints. For the present study a penalty function method is chosen from the wealth of methods available for nonlinear constrained optimization. Penalty methods provide a solution of the constrained problem by means of a sequence of unconstrained minimization problems. We consider the penalty function

$$p = f_s + \Omega(R, \phi_1, \phi_2, \phi_3, \ldots, \phi_M), \tag{15}$$

where the penalty term Ω incorporates the M inequality constraint functions, and R is a fixed constant. The

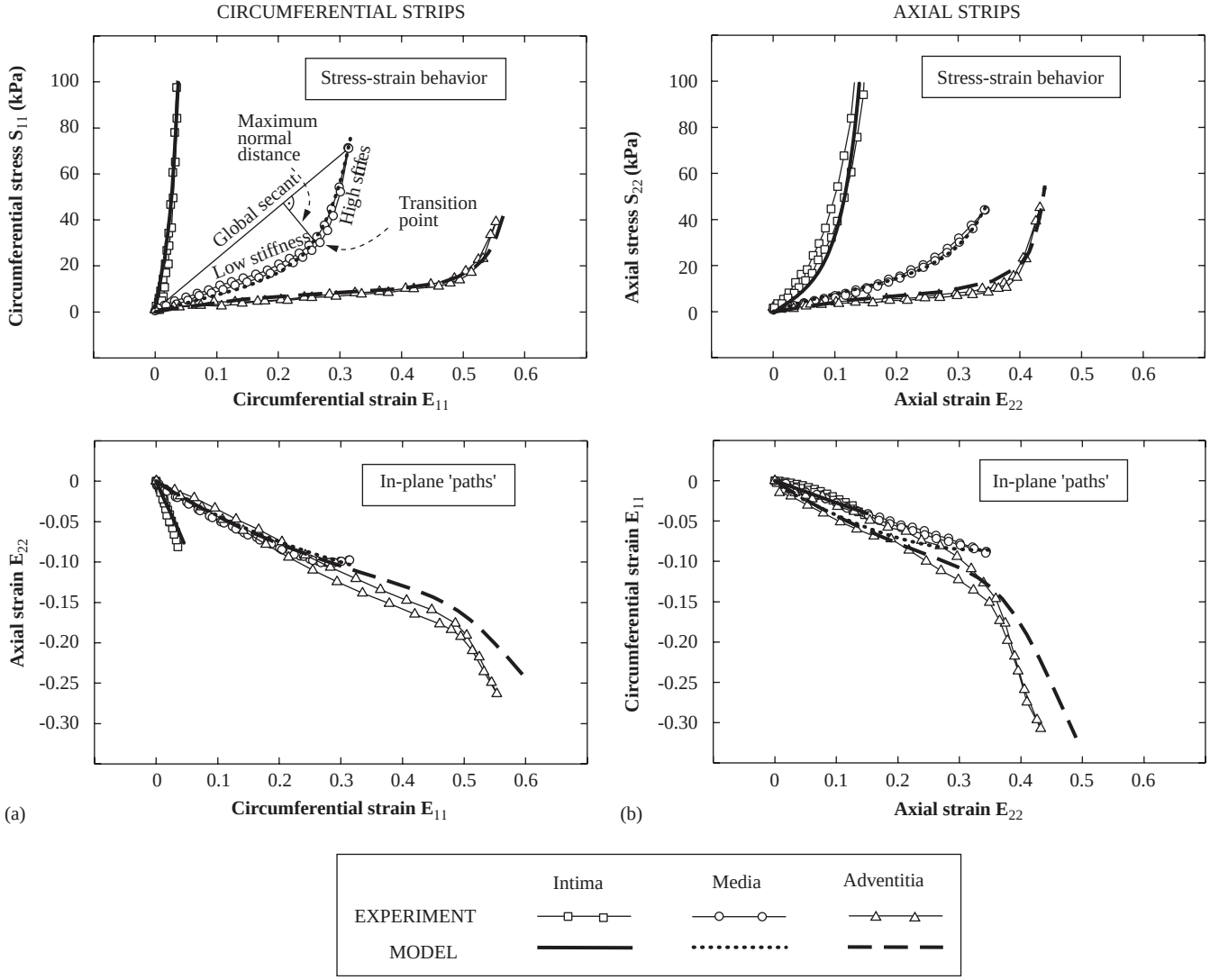

Fig. 5. Uniaxial stress strain behavior (second Piola Kirchhoff stresses S_{11}, S_{22}, and Green Lagrange strains E_{11}, E_{22}), and in plane strain 'paths' obtained from strip samples of isolated aortic layers with (a) circumferential and (b) axial orientations. Thin lines indicate experimental values, while thick lines represent model predictions. Data of the intimal strips are considered only up to tensile stresses of 100 kPa. Determination of the transition point, which separates a low stiffness region from a high stiffness region at the 'knee' of the stress strain curve, is illustrated for the media strip with circumferential orientation (a).

penalty term has to be updated for each minimization step.

A particular penalty function method is Schuldt's algorithm (Schuldt et al., 1977), in which Ω is expressed as

$$\Omega = R\sum_{m=1}^{M}(\langle\phi_m + \sigma_m\rangle^2 - \sigma_m^2), \tag{16}$$

where $\sigma_m \in \{1, 2, 3, \ldots, M\}$ are adjustable parameters associated with the inequality constraints, and the bracket operator $\langle\bullet\rangle$ in Ω symbolizes the rule

$$\langle\bullet\rangle = \begin{cases} \bullet & \forall \bullet \leqslant 0, \\ 0 & \forall \bullet > 0. \end{cases} \tag{17}$$

While R is kept fixed through all stages of the solution, the penalty parameter σ_m is updated after each minimization step according to the rule

$$\sigma_m^{(new)} = \langle\phi_m(C^{(old)}, c_{11}^{(old)}, c_{12}^{(old)}, c_{22}^{(old)}) + \sigma_m^{(old)}\rangle,$$
$$m \in \{1, 2, 3, \ldots, M\}, \tag{18}$$

where the set $\{C^{(old)}, c_{11}^{(old)}, c_{12}^{(old)}, c_{22}^{(old)}\}$ is the solution of the previous minimization step. For the initial step a convenient choice of the set $\{\sigma_1, \sigma_2, \sigma_3, \ldots, \sigma_M\}$ is zero. Since there is no general applicable rule for determining R, appropriate values must be chosen through numerical experiments. For this study the described penalty method was programmed as a Mathematica package. For the unconstrained optimization steps a built-in

Mathematica module was used, which utilizes optionally Brent's method, the Levenberg–Marquardt method, Newton's method and the quasi-Newton method. A new approach for the estimation of an appropriate set $\{C, c_{11}, c_{12}, c_{22}\}$ of start values is presented briefly in the appendix.

4. Results

4.1. Histology and constitutive models

Intimal, medial and adventitial samples showed fiber angles of $18.8^\circ \pm 8.2^\circ$, $37.8^\circ \pm 20.6^\circ$ and $58.9^\circ \pm 14.8^\circ$ (mean ± SD, see Fig. 4), respectively.

The constitutive parameters $\mu, C, c_{11}, c_{12}, c_{22}$ and the fiber angles, φ_{pred} say, *predicted* by the model through Eqs. (7) and (8) for each arterial layer are summarized in Table 3. Note that the predicted (model) fiber angles φ_{pred} for all arterial layers are in relatively good agreement with the mean fiber angles obtained from histological images examined by a histopathologist; this is particularly the case for the intima and the adventitia (compare with Fig. 4). In addition, root mean square errors ε for the circumferential and axial components (ε-S_{11} and ε-S_{22}) of the second Piola–Kirchhoff stress tensor are provided. The error measure is based on the value of the 'objective function' χ^2 of the considered constitutive model, and defined as

$$\varepsilon = \frac{\sqrt{\chi^2/(n-q)}}{S_{ref}}, \tag{19}$$

where n is the number of considered data points, q is the number of parameters of Ψ, and hence $n-q$ is the number of degrees of freedom. The value S_{ref} is the sum of all second Piola–Kirchhoff stresses for each data point divided by the number of all data points. Analogous to the procedure which was used to determine ε-S, the root mean square errors for the circumferential and axial components of the Green–Lagrange strain tensor were computed to be 0.0280, 0.1024 for the intima, 0.0852, 0.0922 for the media, and 0.1208, 0.0998 for the adventitia, respectively.

Plots for the strain energy of the intima, media and adventitia over the in-plane strains E_{11} and E_{22} demonstrate remarkable differences for the layers in stiffness, anisotropy and nonlinearity (see Fig. 6).

4.2. Load-deformation behavior

All three layers show anisotropic responses (compare the stress–strain behaviors for the circumferential and axial strips), with nonlinear stiffening, which is typical for most soft biological tissues; the hystereses are remarkably small (Fig. 5). Additionally, the media and adventitia show soft initial responses, which are similar for both orientations. Despite these common features the layer responses are highly specific. The intima, for example, has the highest global stiffness and the highest degree of anisotropy, while the adventitial response exhibits the most pronounced nonlinearity.

5. Discussion

Constitutive models for soft biological tissues, when based on appropriate mechanical tests, are vital for the

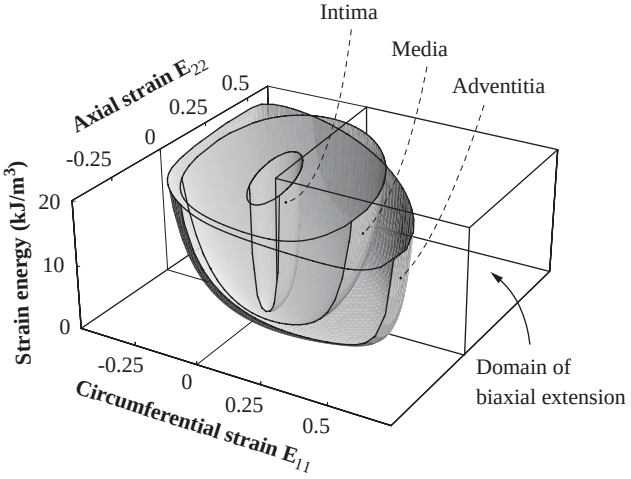

Fig. 6. Strain energy of the three aortic layers plotted over the in plane strains E_{11} and E_{22}. Physiological loading occurs in the region of biaxial extension.

Table 3
Constitutive parameters for the intima, media and adventitia of a human aorta

Layer	μ (kPa)	C (kPa)	c_{11}	c_{12}	c_{22}	φ_{pred} (°)	$\varepsilon\ S_{11}$	$\varepsilon\ S_{22}$
Intima	39.8	1.42	999.0	510.0	127.0	15.2	0.0377	0.1282
Media	31.4	0.140	32.8	14.7	23.5	28.8	0.0526	0.0197
Adventitia	17.3	471.0E 6	37.7	58.0	63.8	57.1	0.0348	0.0523

The fiber angles φ_{pred} predicted by the models are computed through Eqs. (7) and (8). Root mean square errors ε are computed for the circumferential ($\varepsilon\ S_{11}$) and axial ($\varepsilon\ S_{22}$) components of the second Piola Kirchhoff stress tensor according to Eq. (19).

understanding of living matter as a mechanical system. Frequently, however, tests that mimic physiological loading states are difficult or even impossible (Holzapfel et al., 2004a). For such cases, the proposed approach is intended to *approximate* physiological responses with uniaxial data obtained from two strip samples oriented orthogonally to each other. It is also possible to use data from only one strip, which, of course, decreases the predictability, and anisotropy cannot be described. One achievement of this study is to present explicit correlations between the fiber structure and the constitutive parameters of the well-established phenomenological Fung-type model (compare with Eqs. (9) and (10)). Hence, the Fung-type model gets a kind of *pseudo-structural* aspect. This result is based on the assumption to align the fiber direction (mean orientation of collagen or smooth muscle component) with the eigenvector of the strain. The quantitative assessment of three-dimensional orientations of collagen—and (medial) smooth muscle component is still an open problem, related data are rather scarce. In particular, the assumption made in this study regarding the structural fabric in the three layers needs to be analysed in more detail. Despite the seminal work (Canham et al., 1989), in which the three-dimensional structural fabric of the different layers in human coronary arteries are analysed by means of polarizing light microscopy, there is some recent work that makes progress in quantifying the patterns of orientation by using microscopy (Finlay et al., 1995), Section 2 in Holzapfel et al. (2002), small-angle light scattering (Billiar and Sacks, 1997), and suitable image processing tools (Elbischger et al., 2004).

Apart from the shortcomings already discussed, there are additional problems with uniaxial extension tests. For example, the structural integrity of the strips is disturbed at the lateral edges. Cut fibers may retract spontaneously or may be pulled back during strip extension, which could lead to alterations of the tensile responses. Additionally, because of their initial soft responses it is sometimes not easy to insert strip samples to a tensile testing machine without subjecting axial loads. Finally, the composition of a specimen may vary throughout its thickness. This is the case, for example, for adventitias, whose fiber densities are highest at the inner portions. All that leads to uncertainties in the constitutive parameters of the material models. Hence, analyses based on such models have to be interpreted with caution.

In order to validate the predictive capability of the models with respect to physiological loading states, comparisons between data from corresponding multi-axial tests and model responses must be performed, whenever this is feasible. Multi-axial tests could then also be used to show the ability how good the model parameters obtained from fitting uniaxial data can predict multi-axial tests. As pointed out above, many specimens such as multi-component diseased materials and layered organs, do, however, not allow (conventional) biaxial tests, which is a fundamental limitation. For this important class of problems constitutive modeling cannot provide precise determination but only reasonable approximations of the multi-axial behavior. The present approach attempts to make the most of this situation by using a theoretical framework that captures the essential mechanical features of arterial walls by incorporating additional structural information. Despite significant limitations, models determined by means of the proposed approach may provide valuable guidance for biomechanical and mechanobiological research.

The potential of the proposed approach was demonstrated by the example of layer-specific models for a human aorta with non-atherosclerotic intimal thickening. This type of wall thickening is thought to restore the baseline wall stress and differs from an atherosclerotic plaque (Glagov and Zarins, 1989). Preparation tests on different aged human aortas indicated that it was not feasible to obtain intact (leak-free) one-layer tubes of all individual tissues in order to perform inflation and extension experiments. According to the author's knowledge the current data are novel regarding the investigation of all three tissue types, and the use of human specimens. One essential result obtained is the marked mechanical heterogeneity of the different aortic tissues (see Figs. 5 and 6). The present study reveals a remarkable thickness, load-bearing capacity and stiffness of the intimal samples in comparison with the media and adventitia. The intima may, therefore, be regarded as a prominent 'macroscopic' layer which seems to contribute significantly to vascular physiology, and which plays a significant role in controlling vessel structure and function. In the face of these data it becomes clear that approaches, which assume that the artery consists of a (single-layer) homogeneous wall structure, are inappropriate if stress–strain distributions through the wall thickness are of interest. More elaborate studies to identify the mechanical properties and geometrical dimensions of the individual vascular tissues are of pressing need, and were performed in a recent study (Holzapfel et al., 2005b) for human coronary arteries. The importance of the proposed approach in biomedical engineering and clinics becomes evident. For example, we know that the shape of stent struts, which are in contact with the intimal surface, has a strong effect on the stress concentration in the intima and on the clinical outcome after stenting (see, e.g. Pache et al., 2003; Holzapfel et al., 2005a); stent struts may lead to intimal laceration and to endothelial cell denudation (see, e.g., Rogers et al., 1999; König et al., 2002), which is a local effect. Hence, for improving our understanding of the balloon–artery interactions during stent placement and for improving stent designs, it is fundamental to better explore the mechanical properties

and role of the separate arterial layers, in particular of the intimal tissue, which is in contact with a deployed stent.

Note, however, that apart from suitable constitutive models, more reliable stress analyses require additional information on residual strains and in situ pre-stretches for each individual layer. Considering the marked differences in the mechanical properties, the mechanical interplay between the three layers in the intact arterial wall must be mediated by (large) residual deformations related to each arterial layer. Actually, experimental studies on aged human arteries have demonstrated significant layer-specific residual strains in the intact arterial wall, see, e.g. Schulze-Bauer et al. (2002, 2003) for femoral and iliac arteries, respectively.

The form of Ψ, as postulated in Eq. (1) with particularizations in Eqs. (2) and (3), is motivated by the observation that the initial response is comparable to that exhibited by rubberlike solids, which is modeled by the neo-Hookean material. The nonlinear stiffening at high strains, observed in several types of soft biological tissues is modeled suitably by the exponential function, as proposed by Fung and co-workers. The study by Holzapfel and Weizsäcker (1998) show good fits to multi-axial data from rat abdominal aorta. It has also been shown to represent appropriately the extension-inflation response in the physiological domain of aged human iliac arteries (Schulze-Bauer et al., 2003). The two-term model (1)–(3), as originally proposed in Holzapfel and Weizsäcker (1998), has been demonstrated to capture better the passive mechanical behavior of arteries than the pure Fung-type strain-energy function (Schulze-Bauer et al., 2003).

The search for appropriate strain-energy functions that represent material responses of arterial tissues, however, is not yet complete; structural approaches seem to be particularly promising. Holzapfel et al. (2000, 2004b) (with an extension in Holzapfel et al. (2005a)), for example, have proposed a structurally motivated energy function, which, for one family of fibers, has the particular form of

$$\Psi = \Psi_{iso} + \frac{k_1}{2k_2}\{\exp[k_2(I_4-1)^2]-1\}, \tag{20}$$

where the exponential function accounts for the strong stiffening effect of each layer observed at high arterial pressures. Note that the parameters k_1 and k_2 differ from those introduced in Section 2.1. In Eq. (20), $k_1>0$ is a stress-like material parameter and $k_2>0$ is a dimensionless parameter. An appropriate choice of k_1 and k_2 enables the histologically-based assumption that the collagen fibers do not influence the mechanical response of the artery in the low arterial pressure domain to be modeled (Roach and Burton, 1957).

The energy function (20) considers the (mean) orientation of collagen (or smooth muscle component) in the form of the invariant I_4, which is the square λ_f^2 of the fiber stretch (see Eq. (11)). The invariant I_4 can also be expressed as the double contraction $\mathbf{C}:\mathbf{A}$, where $\mathbf{A}=\mathbf{a}_0\otimes\mathbf{a}_0$ is a structure tensor, and $[\mathbf{a}_0]=[\cos\varphi\ \sin\varphi]^{\mathrm{T}}$ is the matrix representation of the direction vector $\mathbf{a}_0$ ($|\mathbf{a}_0|=1$) for the fiber bundle characterized by φ. The anisotropic term in Eq. (20) contributes only when the fibers are extended, i.e. when $I_4>1$. If this inequality condition is taken into account, convexity is guaranteed a priori by the exponential form (20) for an arbitrary set of (positive) material parameters (Holzapfel et al., 2004b). Since the mean angle φ acts as a geometrical parameter, upper and lower limits φ_{u} and φ_{l} for the fiber orientation are provided directly. For more details of the model and related mechanical, mathematical and computational aspects the reader is referred to Holzapfel et al. (2002, 2004b).

Additionally to structural models, advances may still come from phenomenological approaches. Ogden and Schulze-Bauer (2000), for example, have proposed a phenomenological strain-energy function that has been shown to model extension-inflation responses of aged human iliac arteries in a broad load range more efficiently than Fung-type models. Modeling the in vivo constitutive behavior is a challenging task. It requires continuous advances and developments in experimental and theoretical methods tailored to arterial tissues. Appropriate methods will likely have to combine mechanical, structural and biological information. Determination of material models from uniaxial extension tests and histostructural data, as presented in this study, may help to advance constitutive descriptors for arterial walls.

Acknowledgements

The author is indebted to the late Christian A.J. Schulze-Bauer, MD, M.Sc. who suddenly passed away on December 5, 2002. Many of the presented ideas were shaped together with him. The author gratefully acknowledge the support of P. Regitnig, MD from the Institute of Pathology, Medical University Graz, who harvested autopsy specimens, and prepared and analysed the histological sections. The author also thank G. Sommer for his contribution to the experimental tests. Financial support for this research was partly provided by the Austrian Science Foundation under START-Award Y74-TEC. This support is gratefully acknowledged.

Appendix A. Estimation of appropriate start values for the constitutive parameters $C, c_{11}, c_{12}, c_{22}$

The efficiency of multivariate nonlinear regression analysis depends crucially on the choice of appropriate

start values for the constitutive parameters C, c_{11}, c_{12} and c_{22} considered in the function $\hat{\Psi}_{ortho}$, i.e. Eq. (3). The fifth constitutive parameter $\mu > 0$ associated with $\hat{\Psi}_{iso}$, i.e. Eq. (2), is determined by a simple univariate fitting procedure, as described in Section 3.3.

Data on the experimental path can be used to determine the ratios $c_{11} : c_{12} : c_{22}$. For this purpose we provide equations related to the experimental paths $S_{11} = 0$ (strip with x_2-orientation) and $S_{22} = 0$ (strip with x_1-orientation) predicted by the function $\hat{\Psi}_{ortho}(E_{11}, E_{22})$, i.e.

$$S_{11} = \frac{\partial \hat{\Psi}_{ortho}}{\partial E_{11}} = 0, \quad S_{22} = \frac{\partial \hat{\Psi}_{ortho}}{\partial E_{22}} = 0, \tag{21}$$

respectively. As solutions we obtain the linear path $E_{22} = -2c_{11}E_{11}/c_{12}$ for the strip with x_2-orientation ($S_{11} = 0$), and $E_{11} = -2c_{22}E_{22}/c_{12}$ for the strip with x_1-orientation ($S_{22} = 0$). Since the mechanical response in the high-stress domain is mainly governed by $\hat{\Psi}_{ortho}$, the values for $-2c_{11}/c_{12}$ (strip with x_2-orientation) and $-c_{12}/2c_{22}$ (strip with x_1-orientation) can be approximated from experimental data as the respective secants $\kappa_2 = E_{22}/E_{11}|_{S_{22}^{max}}$ (strip with x_2-orientation) and $\kappa_1 = E_{22}/E_{11}|_{S_{11}^{max}}$ (strip with x_1-orientation), where S_{22}^{max} and S_{11}^{max} are the maximum tensile stresses of the related uniaxial extension data. Hence, we deduce a rough estimation that

$$c_{11} : c_{12} : c_{22} = \left(-\frac{\kappa_2}{2}\right) : 1 : \left(-\frac{1}{2\kappa_1}\right), \tag{22}$$

where κ_1 and κ_2 are to be computed from experimental data.

Start values for C and c_{12} can then be determined by taking experimental data for one strip sample. That strip sample should be considered (circumferential or axial), which behaves stiffer under extension. Subsequently, we compute the orthotropic 'Fung-type' strain-energy function $\hat{\Psi}_{ortho}$, i.e. Eq. (3), by means of the work $\hat{W}$ done by the stress field on the strip of unit volume during testing, i.e. Eq. (14), and the isotropic function $\hat{\Psi}_{iso}$, i.e. Eq. (1), according to $\hat{\Psi}_{ortho}(\overline{E}_{11}, \overline{E}_{22}) = \hat{W}(\overline{E}_{11}, \overline{E}_{22}) - \hat{\Psi}_{iso}(\overline{E}_{11}, \overline{E}_{22})$. This equation is now evaluated for two data records: (i) for the strains $\overline{E}_{11} = E_{11}^{max}$, $\overline{E}_{22} = E_{22}^{max}$ which occur at the maximum tensile stress of the related uniaxial extension test, and (ii) for the strains $\overline{E}_{11} = E_{11}^{trans}$, $\overline{E}_{22} = E_{22}^{trans}$ at the 'transition point', as introduced in Section 3.3. In addition, there is a need to check that $\hat{W}(E_{11}^{trans}, E_{22}^{trans}) - \hat{\Psi}_{iso}(E_{11}^{trans}, E_{22}^{trans}) > 0$. This generates two equations for the four unknowns C, c_{11}, c_{12}, c_{22} (note that the constitutive parameter μ is already determined). Two additional equations are used by expressing c_{11} and c_{22} in terms of c_{12} using relation (22). The remaining two equations can then be solved for C and c_{12} so that a complete set of start values is determined.

Remark A.1. Relation (22) may also be helpful for a rough 'consistency check', which is a check to identify the deviation of the used constitutive model from experimental data (provided that the uniaxial extension tests have caused significant stiffening of the specimens).

The identification of the slopes $-2c_{11}/c_{12}$ and $-c_{12}/2c_{22}$ with κ_2 and κ_1, respectively, implies that $c_{12}^2 = 4c_{11}c_{22}\kappa_1/\kappa_2$. By comparing with inequality (5) we find the 'consistency check'

$$\frac{\kappa_1}{\kappa_2} < 1. \tag{23}$$

If experimental data do not satisfy condition (23) one may conclude that either the constitutive model used is inappropriate for the considered type of material or that the response data are flawed due to, for example, bulge of the sample and rotation of markers during extension testing, etc. Finally, the mean angle φ can be estimated by substituting Eq. (8) and the relations c_{11}/c_{12} and c_{12}/c_{22}, which are obtained from Eq. (22), into Eq. (7) to get

$$\tan\varphi = \frac{1}{\overline{\kappa} + (1 + \overline{\kappa}^2)^{1/2}}, \quad \overline{\kappa} = \frac{1 - \kappa_1\kappa_2}{2\kappa_1} \tag{24}$$

and to be solved for φ. A comparison of the result with histostructural data provides another immediate 'consistency check'.

Remark A.2. The 'experimental path' may appear in a variety of characteristic shapes, which depend on the (mean) angle φ, the position of the 'transition point' and the width of a so-called 'transitional zone' in which the material behavior shifts from the 'isotropic path', described by $\hat{\Psi}_{iso}$, to the 'anisotropic path', described

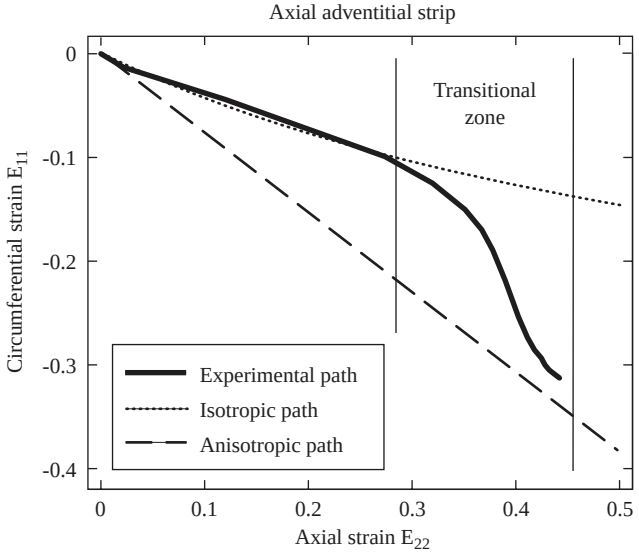

Fig. 7. During extension of an axial adventitial strip from a human aorta with non atherosclerotic intimal thickening the 'experimental (in plane) path' transitions from the 'isotropic path' (described by $\hat{\Psi}_{iso}$) to the 'anisotropic path' (described by $\hat{\Psi}_{ortho}$).

by $\hat{\Psi}_{ortho}$ (see Fig. 7 for an axial strip of the adventitia obtained from a human aorta). The 'isotropic path' for strips oriented and tested uniaxially along, for example, the x_2-axis is governed by the nonlinear function $E_{11} = [(2E_{22} + 1)^{1/2} - 1]/2$, which is the solution of the equation $\partial\hat{\Psi}_{iso}/\partial E_{11} = 0$, while the 'anisotropic path' is governed by function $(21)_1$.

References

Billiar, K.L., Sacks, M.S., 1997. A method to quantify the fiber kinematics of planar tissues under biaxial stretch. J. Biomech. 30, 753 756.

Canham, P.B., Finlay, H.M., Dixon, J.G., Boughner, D.R., Chen, A., 1989. Measurements from light and polarised light microscopy of human coronary arteries fixed at distending pressure. Cardiovasc. Res. 23, 973 982.

Driessen, N.J.B., Wilson, W., Bouten, C.V.C., Baaijens, F.P.T., 2004. A computational model for collagen fibre remodelling in the arterial wall. J. Theor. Biol. 226, 53 64.

Elbischger, P.J., Bischof, H., Regitnig, P., Holzapfel, G.A., 2004. Automatic analysis of collagen fibre orientation in the outermost layer of human arteries. Pattern Anal. Appl. 7, 269 284.

Finlay, H.M., McCullough, L., Canham, P.B., 1995. Three dimen sional collagen organization of human brain arteries at different transmural pressures. J. Vasc. Res. 32, 301 312.

Fung, Y.C., Fronek, K., Patitucci, P., 1979. Pseudoelasticity of arteries and the choice of its mathematical expression. Am. J. Physiol. 237, H620 H631.

Glagov, S., Zarins, C.K., 1989. Is intimal hyperplasia an adaptive response or a pathological process? Observations on the nature of nonatherosclerotic intimal thickening. J. Vasc. Surg. 10, 571 573.

Holzapfel, G.A., 2000. Nonlinear Solid Mechanics. A Continuum Approach for Engineering. Wiley, Chichester.

Holzapfel, G.A., Gasser, T.C., 2001. A viscoelastic model for fiber reinforced composites at finite strains: continuum basis, computa tional aspects and applications. Comput. Meth. Appl. Mech. Eng. 190, 4379 4403.

Holzapfel, G.A., Weizsacker, H.W., 1998. Biomechanical behavior of the arterial wall and its numerical characterization. Comput. Biol. Med. 28, 377 392.

Holzapfel, G.A., Eberlein, R., Wriggers, P., Weizsacker, H.W., 1996. A new axisymmetrical membrane element for anisotropic, finite strain analysis of arteries. Comput. Meth. Appl. Mech. Eng. 12, 507 517.

Holzapfel, G.A., Gasser, T.C., Ogden, R.W., 2000. A new constitutive framework for arterial wall mechanics and a comparative study of material models. J. Elasticity 61, 1 48.

Holzapfel, G.A., Gasser, T.C., Stadler, M., 2002. A structural model for the viscoelastic behavior of arterial walls: continuum formula tion and finite element analysis. Eur. J. Mech. A/Solids 21, 441 463.

Holzapfel, G.A., Sommer, G., Regitnig, P., 2004a. Anisotropic mechanical properties of tissue components in human athero sclerotic plaques. J. Biomech. Eng. 126, 657 665.

Holzapfel, G.A., Gasser, T.C., Ogden, R.W., 2004b. Comparison of a multi layer structural model for arterial walls with a Fung type model, and issues of material stability. J. Biomech. Eng. 126, 264 275.

Holzapfel, G.A., Stadler, M., Gasser, T.C., 2005a. Changes in the mechanical environment of stenotic arteries during interaction with stents: computational assessment of parametric stent design. J. Biomech. Eng. 127, 166 180.

Holzapfel, G.A., Sommer, G., Gasser, C.T., Regitnig, P., 2005b. Determination of the layer specific mechanical properties of human coronary arteries with non atherosclerotic intimal thickening, and related constitutive modelling, in press, doi:10.1152/ajpheart.00934.2004.

Konig, A., Schiele, T.M., Rieber, J., Theisen, K., Mudra, H., Klauss, V., 2002. Influence of stent design and deployment technique on neointima formation and vascular remodeling. Z. Kardiol. 91, 98 102.

von Maltzahn, W. W., Warriyar, R.G., Keitzer, W.F., 1984. Experi mental measurements of elastic properties of media and adventitia of bovine carotid arteries. J. Biomech. 17, 839 847.

von der Mark, K., 1981. Localization of collagen types in tissues. Int. Rev. Conn. Tiss. Res. 9, 265 324.

Menzel, A., 2005. Modelling of anisotropic growth in biological tissues. A new approach and computational aspects. Biomech. Model. Mechanobio. 3, 147 171.

Ogden, R.W., 1997. Non linear Elastic Deformations. Dover, New York.

Ogden, R.W., 2003. Nonlinear elasticity, anisotropy, material stability and residual stresses in soft tissue. In: Holzapfel, G.A., Ogden, R.W. (Eds.), Biomechanics of Soft Tissue in Cardiovascular Systems. CISM Courses and Lectures No. 441, International Centre for Mechanical Sciences, Springer, Wien, pp. 65 108.

Ogden, R.W., Schulze Bauer, C.A.J., 2000. Phenomenological and structural aspects of the mechanical response of arteries. In: Casey, J., Bao, G. (Eds.), Mechanics in Biology, vol. 242/BED vol. 46. The American Society of Mechanical Engineers (ASME), New York, pp. 125 140.

Pache, J., Kastrati, A., Mehilli, J., Schuhlen, H., Dotzer, F., Hausleiter, J., Fleckenstein, M., Neumann, F.J., Sattelberger, U., Schmitt, C., Muller, M., Dirschinger, J., Schomig, A., 2003. Intracoronary stenting and angiographic results: strut thickness effect on restenosis outcome (ISAR STEREO 2) trial. J. Am. Coll. Cardiol. 41, 1283 1288.

Pedersen, P., 1989. On optimal orientation of orthotropic materials. Struct. Optim. 1, 101 106.

Roach, M.R., Burton, A.C., 1957. The reason for the shape of the distensibility curve of arteries. Canad. J. Biochem. Physiol. 35, 681 690.

Rogers, C., Tseng, D.Y., Squire, J.C., Edelman, E.R., 1999. Balloon artery interactions during stent placement: a finite element analysis approach to pressure, compliance and stent design as contributors to vascular injury. Circ. Res. 84, 378 383.

Schuldt, S.B., Gabriele, G.A., Root, R.R., Sandgren, E., Ragsdell, K.M., 1977. Application of a new penalty function method to design optimization. ASME Trans., J. Eng. Ind. 99, 31 36.

Schulze Bauer, C.A.J., Regitnig, P., Holzapfel, G., 2002. Mechanics of the human femoral adventitia including high pressure response. Am. J. Physiol. Heart Circ. Physiol. 282, H2427 H2440.

Schulze Bauer, C.A.J., Morth, C., Holzapfel, G.A., 2003. Passive biaxial mechanical response of aged human iliac arteries. J. Biomech. Eng. 125, 395 406.

Wilber, J.P., Walton, J.R., 2002. The convexity properties of a class of constitutive models for biological soft tissues. Math. Mech. Solids 7, 217 235.